Lab on a Chip

Microfluidics for Electrophysiology, Imaging, and Behavioral Analysis of Hydra

Journal:	*Lab on a Chip*
Manuscript ID	LC-ART-05-2018-000475.R2
Article Type:	Paper
Date Submitted by the Author:	30-Jun-2018
Complete List of Authors:	Badhiwala, Krishna; Rice University, Department of Bioengineering Gonzales, Daniel; Rice University, Department of Electrical and Computer Engineering; Applied Physics Program Vercosa, Daniel; Rice University, Department of Electrical and Computer Engineering; Applied Physics Program Avants, Benjamin; Rice University, Department of Electrical and Computer Engineering Robinson, Jacob; Rice University, Department of Electrical and Computer Engineering; Department of Bioengineering;

Microfluidics for Electrophysiology, Imaging, and Behavioral Analysis of *Hydra*

Krishna N. Badhiwala[1], Daniel L. Gonzales[2,3], Daniel G. Vercosa[2,3], Benjamin W. Avants[2], Jacob T. Robinson*[1,2,4,]

1. Department of Bioengineering, Rice University, 6100 Main Street, Houston, Texas 77005
2. Department of Electrical and Computer Engineering, Rice University, 6100 Main Street, Houston, Texas 77005
3. Applied Physics Program, Rice University, 6100 Main Street, Houston, Texas 77005
4. Department of Neuroscience, Baylor College of Medicine, One Baylor Plaza, Houston, Texas, 77030

*Correspondence to: jtrobinson@rice.edu.

ABSTRACT

The nervous system of the cnidarian *Hydra vulgaris* exhibits remarkable regenerative abilities. When cut in two, the bisected tissue reorganizes into fully behaving animals in approximately 48 hours. Furthermore, new animals can reform from aggregates of dissociated cells. Understanding how behaviors are coordinated by this highly plastic nervous system could reveal basic principles of neural circuit dynamics underlying behaviors. However, *Hydra's* deformable and contractile body makes it difficult to manipulate the local environment while recording neural activity. Here, we present the first microfluidic technologies capable of simultaneous electrical, chemical, and optical interrogation of these soft, deformable organisms. Specifically, we demonstrate devices that can immobilize *Hydra* for hours-long simultaneous electrical and optical recording, and chemical stimulation of behaviors revealing neural activity during muscle contraction. We further demonstrate quantitative locomotive and behavioral tracking made possible by confining the animal to quasi-two-dimensional micro-arenas. Together, these proof-of-concept devices show

that microfluidics provide a platform for scalable, quantitative cnidarian neurobiology. The experiments enabled by this technology may help reveal how highly plastic networks of neurons provide robust control of animal behavior.

INTRODUCTION

Understanding the relationship between animal behavior and the activity of individual cells in the nervous system is one of the fundamental goals in neuroscience. To reach this goal, scientists are developing new electrical and optical technologies capable of simultaneously recordings from hundreds of individual neurons with the temporal resolution to capture individual action potentials.[1–15] These technologies, however, fall well short of recording every action potential from each individual neuron in vertebrate model organisms that have neurons numbering from the hundreds of thousands to tens of billions.

Thus, to observe cellular level activity of the entire nervous system, scientists often turn to small invertebrates like *Caenorhabditis elegans* and *Drosophila melanogaster*. In addition to having far fewer neurons, their small size and transparency facilitates in vivo calcium- or voltage-sensitive fluorescence imaging that can record simultaneous activity of hundreds to thousands of individual neurons.[11,16–19] To make these investigations even more attractive, several lab-on-a-chip technologies now provide increased throughput for chemical, optical, and electrical interrogation of *C. elegans* and *D. melanogaster* on microfluidic platforms. This confluence of technologies has revealed how many behaviors can be implemented by neural circuits,[20–24] however, *C. elegans* and *D. melanogaster* may not be the best suited to study neural circuit repair and remodeling. Although neurites connecting cells can regrow when severed, if even a single neuron is ablated, *C. elegans* or *D. melanogaster* often show significant and permanent behavioral deficits.[21,23,25–31] This static and fragile neural architecture stands in stark contrast to the mammalian cortex, which can remodel itself to retain or regain function despite the loss of a significant number of neurons.[32–34]

In contrast to *C. elegans* and *D. melanogaster*, the architecture of the *Hydra* nervous system is extremely dynamic making it an exciting model for studying neural plasticity and repair. While the *Hydra* are small (0.5 – 15 mm in length) and transparent like *C. elegans* and *D. melanogaster* larvae, the entire population of neurons in *Hydra* nervous system is continually replenished allowing animals to regenerate after being cut into several pieces and even reform from aggregates of dissociated cells.[35,36]

Hydra are also a compelling model organism because their diffuse network of spiking neurons resembles neural network models often studied by computational neuroscientists.[37] For example, *Hydra* have several genes that encode voltage-gated ion channels allowing their neurons to generate fast action potentials similar to those in mammalian nervous systems.[38] Genomic analysis show the presence of gap junctional proteins as well as common neuropeptides and neurotransmitters.[39–43] Ultrastructural studies show evidence of both chemical and electrical synapses.[44–46] Thus, unlike *C. elegans*, whose neurons lack sodium driven action potentials, *Hydra* (like *D. melanogaster*) have genes encoding for voltage-gated sodium channels and thus provides opportunities to study information processing in simple networks of spiking neurons.

While the small size of *Hydra* offers several advantages as a model organism, it also presents challenges for moving and manipulating the organism, performing simultaneous electrophysiology and imaging, and delivering well-controlled stimuli. Previously reported immobilization techniques have several limitations that make such multi-modal interrogation difficult.[47,48] Previously, simultaneous electrophysiology and imaging has been limited to dissected animals due to contractile movements, and typical recordings last only few seconds.[48] While chemical stimulation is possible with flow cell coverslip preparations, the lack of physical immobilization to keep animals in the microscope field of view makes it difficult to maintain cellular resolution optical imaging. In the case of *D. melanogaster* and *C. elegans* that are similarly sized, this challenge has been addressed using microfluidic technology.[49–51] Microfluidics provides robust and scalable methods to reversibly restrain and physically manipulate *D. melanogaster* [52–56] and *C. elegans.*[57–67] Specifically, in the case of *C. elegans,* microfluidics have been shown to provide precise

control over the local environment for observing taxis and locomotive behaviors, performing calcium imaging and recording electrophysiological activity from the pharynx and body-wall muscles.[22,61,65,68–71]

Unfortunately, direct application of the existing microfluidic technologies is unlikely to succeed for *Hydra* due to the animal's soft and deformable body. While previous work have shown that *Hydra* can be held in place by sealing the animal between coverslips or flexible membranes,[47,48] we have found no reports of immobilization strategies that include microfluidic channels that enable chemical perfusion, adding or removing animals, and multi-day experiments. Here we show that with appropriate design and operation, microfabricated fluidic devices allow scalable and customizable solutions for multi-modal interrogation of these soft deformable animals. Unlike *C. elegans* and *D. melanogaster*, *Hydra* has neither a tough protective cuticle nor a stereotyped size. Miniscule forces, on the order of nano-newtons, are sufficient to tear the epithelial cell layers to form an oral cavity. Body contractions themselves can generate forces of this magnitude.[72] Thus, the spontaneous body contractions and elongations can shear and dissociate the epithelia, if the aggressive microfluidic confinement strategies successful in small invertebrates like *C. elegans* are translated directly to *Hydra*. Furthermore, within a clonal population, *Hydra* may vary in size by more than a factor of ten and an individual animal can change length by an order of magnitude during contraction. Thus, any microfluidic confinement or immobilization strategy must accommodate deformable animals of a variety of sizes and reduce shear forces.

Here we show that specially designed microfluidic devices enable key neurobiological experiments to be performed in *Hydra*. Specifically, we illustrate safe handling and manipulation of the gelatinous *Hydra* in a microfluidic environment for several hours to days by carefully controlling fluidic pressure. We also show how the microfluidic devices allow us to use electrical and optical techniques to simultaneously measure the activity of muscle cells and the group of neurons responsible for motor function during body column longitudinal contractions. We can also stimulate specific behaviors, such as feeding, by using chemical stimulants to study the cellular level activity at the onset and during the behavior. We also replicate and quantitatively analyze a subset of the *Hydra* behaviors in the microfluidic arena essential for behavioral

and locomotion assays. To our knowledge, this is the first microfluidic platform for manipulating entire *Hydra* for simultaneous imaging, electrophysiology, and scalable behavioral studies.

RESULTS AND DISCUSSION

Manipulation and immobilization of *Hydra* in microfluidic devices

Despite the soft and deformable body of the *Hydra,* we found that with care, we could transfer the animal into and out of the microfluidic devices with roughly 95% success (Fig. 1a,b, Supplementary Movie 1). To load *Hydra* into a microfluidic device, we use a transfer pipette to move an animal into an open syringe cap connected to the device via tygon tubing. Because *Hydra* readily attach themselves to many surfaces, we found that drawing the animal into the tygon tubing quickly dramatically improved the success of loading. Once loaded, the animal's position can be precisely controlled with gentle application of fluid flow. Unloading follows a similar procedure in reverse (see Methods).

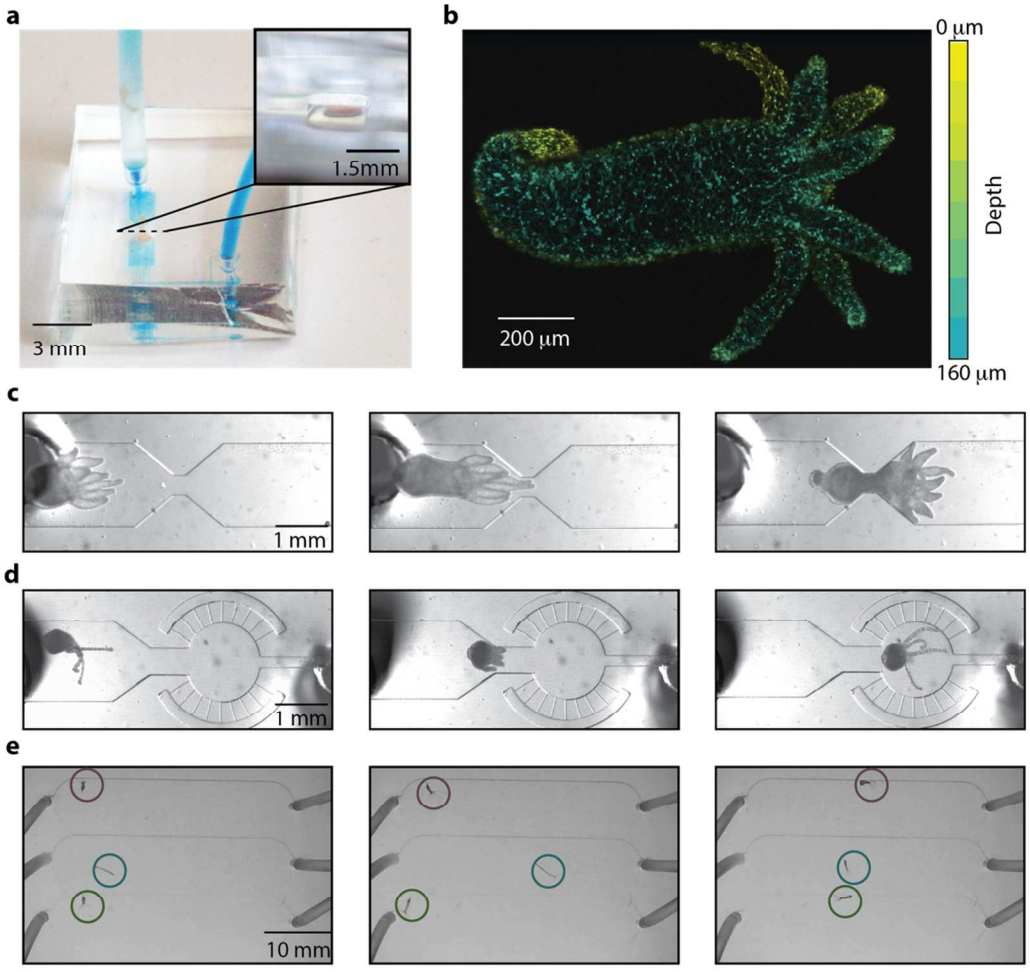

Figure1: Microfluidic Manipulation and Immobilization of *Hydra*. (a) Typical *Hydra*, 0.5 mm in diameter, is immobilized in a 110 μm tall hour-glass microfluidic chamber (shown with blue dye). The tubing inserted in the inlet port is near the top of image (with a *Hydra* in it for demonstration purpose) and tubing inserted in control port is shown towards the bottom right. For *Hydra* immobilization and size comparison, inset on the right shows zoom-in of a cross-section of microfluidic chamber with similar sized flattened *Hydra*. **(b)** Maximum fluorescence intensity projection image shows *Hydra* nerve net with the colors (yellow to teal) corresponding to the depth (from z-stack taken with confocal microscopy). *Hydra* with pan-neuronal expression of GFP under actin promoter was immobilized in a 160 μm tall microfluidic chemical interrogation chamber (wheel-and-spoke geometry shown in (d)) and anesthetized with 0.1% chloretone on-chip prior to imaging. **(c-d)** Optical micrographs show loading (left), habituation (middle) and precise positioning of *Hydra* (right) in different microfluidic chambers: **(c)** hour-glass chamber for electrophysiology constraining the body column from large movements; **(d)** wheel-and-spoke perfusion chamber constraining locomotion; **(e)** behavioral micro-arena with three separate 7 mm wide and 600 μm tall channels for high-throughput behavioral imaging of non-interacting *Hydra*. Circles indicate the positions of behaving *Hydra* in the micro-arena.

To showcase how microfluidics enable a variety of *Hydra* studies ranging from electrophysiology to quantitative analysis of locomotion, we created three classes of immobilization chambers: 1) hour-glass shaped chambers that reduce *Hydra* movement for high-resolution cellular imaging and electrophysiology (Fig. 1c); 2) wheel-and-spoke geometries that confine *Hydra* to a region roughly the size of the animal to facilitate imaging and chemical perfusion (Fig. 1d); 3) open-field geometries that allow *Hydra* to move and explore a quasi-2D environments (Fig. 1e). For each immobilization chamber, we performed proof-of-principle experiments to demonstrate how these devices can help study *Hydra* neural activity and/or behavior.

Electrophysiology and imaging of immobilized *Hydra*

The hour-glass tight confinement chambers immobilize the animal against the walls of the microfluidic device allowing us to minimize *Hydra* movement for *both* high-resolution optical imaging *and* cellular-scale electrophysiology using nano-SPEAR electrodes that protrude from the walls of the microfluidic channels.[71] These hour-glass chambers effectively immobilize the animal by first flattening the deformable *Hydra* in the roughly 110 μm tall microfluidic channels and then pinch a portion of the mid-body column of the animal to keep it immobile (Fig. 1c). We found that these chambers confined the movement of *Hydra* such that the average movement of the body column was approximately 65 μm/minute (approximately four times less than the movement without confinement), though the tentacles were largely free to move (see methods). A major advantage of these hour-glass shaped immobilization chambers (based on previously reported immobilization chambers for *C. elegans)*[58,71] is that they avoid sharp corners that can damage the soft *Hydra* body and they can accommodate the large differences in animal sizes found in the *Hydra* colonies (Fig. 1c). To our knowledge, this is the first simultaneous calcium imaging and electrophysiology to be performed simultaneously in intact *Hydra*.

Using our unique ability to perform simultaneous electrophysiology and imaging in intact *Hydra,* we sought to identify the origin of the electrical signals recorded from the *Hydra* body. The *Hydra* body is mostly comprised of two layers of contractile epitheliomuscular cells (20-40μm in length) capable of

generating action potentials and innervated by a smaller number of neurons (8-10μm) that also are believed capable of generating action potentials.[73] Using this tight confinement device, we were able to record electrical activity from a single animal for 10 hours using nano-SPEAR electrodes. In these recordings, we observed a mixture of high and low amplitude electrical spikes (Fig. 2b). We then performed simultaneous brightfield imaging in *Hydra vulgaris* AEP for 1 hour under dark conditions, and observed statistically significant correlation between body contractions and electrical spikes recorded with our nano-SPEARs (see large amplitude spikes, Fig. 2c). Statistical significance is determined from 99% confidence interval computed from distribution of correlation values for randomly shuffled data (see methods and Supplementary Fig. 2). Our observed correlation suggests that the electrical signals primarily represent action potentials generated by the muscle cells, which is consistent with previous recordings using nano-SPEAR electrodes in *C. elegans.*[71] To quantify the body and tentacle contractions, we measured the area occupied by the *Hydra* in the upper and lower halves of the microscope image (body size). We found that the majority of small amplitude electrical spikes coincided with tentacle contractions (or small amplitude changes in size of the upper body half). Occasional small amplitude spikes were also observed in the absence of obvious body or tentacle contractions. It is possible that future work could determine if these small amplitude spikes arise from noise or artifacts, or if they represent electrical activity from cells not associated with contractions. The large amplitude waveforms coincided with body contractions bursts (CB) (or large amplitude changes in the size of both the top and bottom halves of the animal) (Fig. 2c) (Supplementary Movie 2). This pattern of small and large amplitude waveforms was observed across six individual animals (Supplementary Fig. 1). Together, the absence of high amplitude electrical activity during body-elongations, when the rhythmic potential (RP) neurons are thought to be active,[48] and large percentage of electrical activity measured during body or tentacle contractions further indicates nano-SPEAR electrodes predominantly measure ectodermal muscle activity associated with body or tentacle contractions. We performed the same analysis on a second animal and observed the same statistically significant correlations between muscle activity and electrical recordings (Supplementary Fig. 3).

Having determined that the electrical signals recorded from our nano-SPEAR electrodes represent muscle activity, we then looked for the neural activity patterns that drive muscle contractions. By performing simultaneous electrophysiology of the muscle cells and calcium imaging in neurons (using a transgenic strain that expresses GCaMP6s pan-neuronally), we could correlate neuronal activity with muscle contractions. When we compared this simultaneously recorded muscle and neuronal activity, we found statistically significant correlation between neural activity and electrical measurements during body contractions (consistent with previous reports[48]) (Fig. 2d, Supplementary Fig. 4). Specifically, during body column contractions, calcium imaging showed synchronous firing of the cluster of neurons in the nerve ring in the animal's foot. Synchronized with this calcium activity, we recorded large amplitude electrical spikes from the epithelial muscle cells (Supplementary Movie 3). Computing the cross-correlation between calcium-sensitive fluorescence imaging and electrophysiology during contractions shows that the neurons in the foot indeed have statistically significant correlation with electrical measurements and body contractions (see significance test in methods) (Fig. 2d). All tentacles also contract during contraction bursts and we also observe statistically significant correlation between large-amplitude electrical spikes and the activity of neurons located near the base of the tentacles. Interestingly, when the body column is elongating or stationary we find no statistically significant correlation between neural activity and electrically-detected muscle activity (Supplementary Fig. 4). Thus, the RP neurons that are active during elongation appear unassociated with any muscle activity (Fig. 2d, right) suggesting that they may play a role in inhibiting body column contraction. During these periods, we often measure isolated, very low amplitude spikes in the electrical activity though neither the pattern nor the timing was correlated well with RP neuronal activity (Fig. 2d, right). We performed the same analysis on a second animal and observed the same statistically significant correlations between muscle activity, electrical recordings, and calcium imaging (Supplementary Fig. 5).

We found that for the hour-glass immobilization chamber, electrophysiology experiments could last between 1 and 10 hours depending on the experimental conditions allowing us to observe many cycles of contraction and elongation. The excitation light used for fluorescence imaging stimulated inchworm-like locomotion away from the recording site and as a result typical imaging experiments could last roughly

one hour. Under low-light conditions during electrophysiology experiments, the animal was much less motile, and experiments could typically last more than 10 hours.

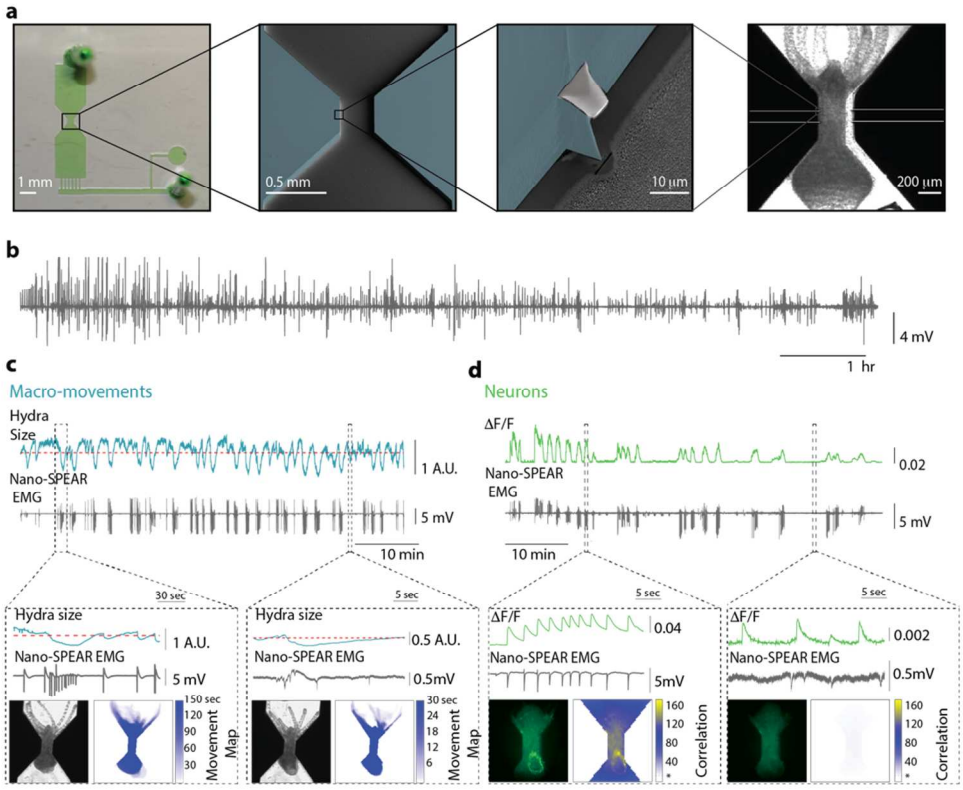

Figure 2: Simultaneous electrophysiology and calcium imaging. (a) Photograph (left) of a microfluidic immobilization chamber filled with green dye. Black box highlights the recording region in the microfluidic chamber (110 µm tall). False colored scanning electron micrograph (middle) shows the recording region (blue, photoresist; light grey, Pt; dark grey, silica) on the nano-SPEAR chip (50 µm tall). Inset shows a zoom-in of the Pt electrode (light grey) suspended mid-way between the top and bottom of the photoresist sidewall(blue). Optical micrograph (right) shows *Hydra* immobilized in the microfluidic chamber placed on top of the nano-SPEAR chip with combined 160 µm tall recording region. **(b)** Representative 10-hour--long electrophysiology trace measured from *Hydra* vulgaris AEP. **(c, d)** Simultaneous electrophysiology and imaging from (**c**) *Hydra* (H. Vulgaris AEP) and (**d**) neurons in transgenic

Hydra (GCaMP6s, neurons) (n=1). Top trace shows c) change in body size (area) of the top half of the *Hydra* body (10 Hz) and (d) mean fluorescence (ΔF/F) neurons (20Hz). Bottom trace shows simultaneously recorded electrical activity from the muscles using nano-SPEARs electrode (1KHz). Left box show correlation during high activity period, contraction burst (c, d). Right box shows correlation during low activity period, (c) tentacle activity or (d) RP-like activity. Within each box, top traces show (c) change in body size, (minima in body size trace means contractions) or (d) peaks in fluorescence (during contractions) coinciding with peaks in electrophysiology (bottom trace). (c) A representative micrograph (left) of *Hydra* shows representative body size. The movement map (left) shows the body regions moving during the period. (d) A representative fluorescence micrograph (left) shows calcium levels with high fluorescence. Spatially-resolved correlogram (right) shows the activity from region in *Hydra* body with high correlation with electrophysiology. Dashed line on the color bar (*) indicates the threshold for statistically significant correlation values (99% confidence interval) determined from shuffled data. Note the pixels overlapping with *Hydra* have high correlation values (blue, yellow) and the background pixels also appear to have statistically significant correlation values (blue) despite not overlapping with *Hydra* body. These pixels show correlation with contractions due to light scattering into the microfluidic chamber and the elevated calcium fluorescence during contractions.

Chemical stimulation of *Hydra* in microfluidics

Chemical stimulation is key tool for neurobiologists allowing them to trigger precisely timed behaviors or to investigate the role of neuromodulators and/or ion channels using known agonists or blockers. To apply chemical stimulation to *Hydra* without stimulating a mechanical response to changing fluid flow rates, we developed 160 μm tall wheel-and-spoke perfusion chambers (Fig. 1d, 3). A key design element of these chambers is a slow perfusion rate that avoids stimulating natural responses to changing fluidic pressures or shear stress. We found that high flow velocities in large microfluidic channels often initiated body contractions or tentacle swaying. At times, high flow rates produced shear forces that damaged *Hydra*. We also observed that *Hydra* would frequently bend or translocate in the direction of the flow. Thus, to apply chemical stimuli without initiating these behaviors, we created microfluidic devices that

minimize the flow rates of chemical stimuli. To minimize the rate of fluid flow into the *Hydra* observation chamber, we relied on the large fluidic resistance created by short and narrow (25 x 20 μm) perfusion channels leading into the larger observation chamber (1500 radius x 160 height, μm). This geometry is based on the previously reported chemical perfusion chambers for perfusion in cell culture arrays.[74]

Proof-of-concept experiments show that perfusion through our wheel-and-spoke chambers induce chemically stimulated behaviors. During 30-minute periods of no fluid flow (I), *Hydra* media flow (0.02mL/min) (II), reduced glutathione (GSH) flow (0.02mL/min) (III), and recovery with *Hydra* media flow (0.02mL/min) (IV), we observed feeding responses as expected with exposure to GSH but no change in behavior during *Hydra* media flow. When we perfused *Hydra* media through our chemical stimulation chamber, we observed minimal change in contraction rate or bending suggesting that the flow rates were sufficiently low to prevent mechanical stimulation (Fig. 3a-c II). Contractions and elongations were quantified by measuring the decreases and increases in body length, respectively (see methods). The continuation of this periodic body contractions and elongations pattern during flow indicated the perfusion flow rates caused negligible mechanical stimulation.

Because the low fluid flow rates engineered in our wheel-and-spokes chambers do not significantly affect *Hydra* behavior, we were able to perfuse GSH (9μM) to induce a feeding response and inhibit body contractions (Fig. 3a-c III). Normal body contractions were interrupted after approximately 15-20 minutes of GSH flow as seen by the lack of sharp decreases in body length as expected through previous reports[75] (Fig. 3c III) and followed by tentacle writhing (Fig. 3b III, top). During tentacle writhing, body length remained constant but tentacles contracted and curled towards the mouth until the oral cavity was formed (Fig. 3b III, bottom). Once the oral cavity had formed, epithelium began folding outwards increasing the mouth size until *Hydra* lost its tubular shape and hydrostatic rigidity (Supplementary Movie 4). The chemically induced response in *Hydra* was then reversed by switching the perfusion input from GSH to *Hydra* media. In all three trials, we successfully recovered the contractile activity as seen by the return of spikes in the body length of *Hydra* (Fig. 3c IV). In all trials, except one, the folded *Hydra* body eventually regained its tubular shape by resealing the oral cavity through the duration of the trial.

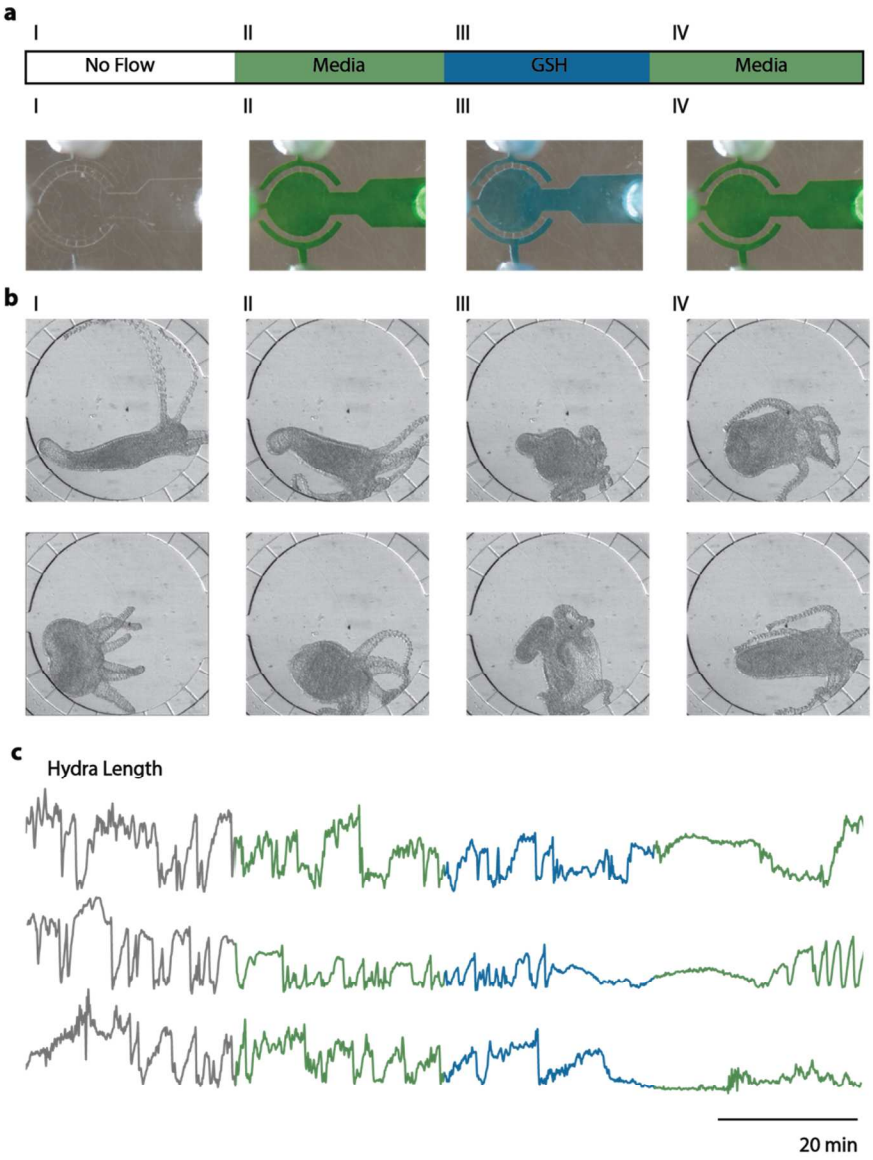

Figure 3: Functional imaging during chemically induced feeding behavior with reduced glutathione (GSH). **(a)** Photographs show a microfluidic chamber with a circular observation chamber in the middle surrounded by small perfusion channels. The narrow perfusion channels with a port on the top and bottom are used for perfusion inflow (0.02mL/min) and outflow, respectively. The dye colors indicate flow conditions: (I) no flow (clear or grey); (II) flow of *Hydra* media (green); (III) 9μM GSH (blue); (IV) *Hydra* media (green). **(b)** micrographs of immobilized *Hydra* show representative activity: (I, II) stereotypical body elongations (top) and contractions (bottom) with no perfusion flow or with media flow; (III) feeding response induced by perfusion of GSH leading to tentacle writhing (top) and outward folding of the epithelia from mouth opening (bottom); (IV) Recovery of typical body contractions (top) and elongations (bottom) following perfusion of *Hydra* media. **(c)** Body length traces (see methods) show contractions and elongations from three individual *Hydra* (colors correspond to flow conditions I-IV). Minimum body length indicates contraction.

The ability to chemically stimulate *Hydra* feeding responses in microfluidic chambers provides the exciting opportunity to image neural activity during these behavioral state transitions. As an example, we imaged neuronal activity in transgenic *Hydra* (GCaMP6s, neurons) under GSH stimulation of the feeding response. To reduce the effects of photobleaching we imaged *Hydra* for five minutes under the flow of *Hydra* media, followed by thirty minutes of GSH, and a second thirty-minute period of *Hydra* media flow (Supplemental Movie 5). We observed that during GSH stimulation, normal body contractions were interrupted and the cluster of neurons in the foot became less active after approximately twenty minutes of GSH flow (Supplementary Movie 5). The neurons at the base of tentacles were active during tentacle writing and the neurons in the upper half of the body seemed more active during mouth opening. During the recovery period with *Hydra* media flow, we initially observed a smaller subset of neurons in the lower half of the body become active but did not lead to body contractions until larger ensemble of neurons in the foot, likely belonging to contraction burst circuit, became active. This ability to perform cellular-resolution imaging during chemically stimulated behaviors provides new opportunities to study sensory-motor transformations in the entire network of spiking neurons in *Hydra.*

Behavioral Analysis of *Hydra* in microfluidics

The quasi-2D environment provided by microfluidics also helps us quantitatively track *Hydra* locomotion and body posture of multiple animals while preventing them from interacting with each other. In addition to periodic body contractions and elongations, *Hydra* can also explore their environment by bending and swaying or move to new locations through inch-worm, somersault or swimming locomotion. Because microfluidic arenas reduce *Hydra* movements to a quasi-2D plane, the task of quantifying *Hydra* movements and posture is greatly simplified and we can use a simple, low-cost camera placed above the device.

Microfluidics also provides an excellent platform for controlling chemical, thermal, and physical conditions. The combination of behavioral tracking and well-regulated environmental conditions will help reveal

sensory-motor processing in these simple neural networks. It may also be possible to combine scalable imaging afforded by microfluidics shown here with machine learning algorithms recently used to classify *Hydra* behaviors.[76]

We found that in microfluidic devices with channel heights ~ 200 - 600 μm *Hydra* display similar behaviors to unrestrained animals in 3D including contraction, elongation, swaying, as well as inch-worm and floating locomotion.[76] Based on our observations of *Hydra* (n=3) over several hours in our parallel 600 μm tall behavioral arenas (Fig. 1e), we classified the *Hydra* behavior into two broad behavioral classes: exploration and locomotion (Fig. 4a,b). We found that just like in flask cultures, *Hydra* in our behavioral arenas typically anchors itself to the top or bottom surface with its foot while periodically contracting and elongating (Supplementary Movie 6). Less frequently, we observed swaying or bending, which is also seen in flask cultures. In addition to these exploratory behaviors we also observed *Hydra* locomotion by either inchworming or floating. We did not observe somersaulting as has been reported in 3D environments[77], perhaps due to the short height of the quasi-2D chamber or the relative rarity of somersaulting events.

By reducing body posture and locomotion to 5 variables, we could quantify *Hydra* behavior over several days (Fig. 4). We defined the change in body length of *Hydra*, L, which allows us to easily detect body contraction events (Supplementary Fig. 6). Because of the low imaging frame rates used, we identified contraction burst (CB) events rather than individual contraction burst pulses (Fig. 4c). On average, we measured similar rate of 9 -15 CBs per hour as previously reported.[78] We defined body orientation as α, the angle of a vector from the foot to the mouth with respect to the positive x-axis. However, we noted that body column of *Hydra* often curved. The body orientation, α, did not represent the direction of the mouth especially when *Hydra* body formed a U-loop. Thus, we obtained body posture by fitting two vectors separated along the midpoint in the body column from the foot to the center of the body and from center of the body to the mouth, α_1 and α_2. The difference between these two angles, β, provided information about the curvature along the body column. In cases when the body column was straight, β was nearly zero. When the body column had slight curvature, there was a small difference between α_1

and $\alpha_2, \beta < \pi/3$. Similarly, when *Hydra* body looped to form U-shape, the angular difference between the two vectors was large, $\pi > \beta >= \pi/3$ (Fig. 4b). Alternatively, comparing the difference in body length based on the Euclidean distance between the mouth and foot either with or without accounting for the body center further confirmed the bending events. Thus, by segmenting the *Hydra* body, we were able to gain additional information about the body postures and exploratory behavior.

Using the time-averaged location of the foot (see Methods) for generating the movement track of *Hydra* through the microfluidic arena, we found the displacement events were significantly less frequent compared to the body contractions (N=3 animals, 60 hours, p-value<0.01, one-sided, unpaired two-sample student's t-test with unequal variances) (Fig. 4d, Supplementary Fig 6d). *Hydra* periodically contracts and elongates in various directions while the foot is anchored to a single location. Translocation occurs when the *Hydra* releases the foot and reattaches it at a different location. Thus, tracking the location of the foot shows the locomotion pattern (Fig. 4c) of *Hydra* where the distance, d, and the direction traveled, γ, are represented by the lines on the track. The locomotion steps were frequently stereotyped inchworm movements where *Hydra* expanded its tentacles and contracted the rest of the body towards the tentacles. *Hydra* was also seen bending over its tentacles to complete the locomotion step. Often *Hydra* took several steps before reattaching the foot. For simplicity, we identified the position where the *Hydra* foot finally adhered as the step final position to determine the locomotion step size and direction (Fig. 4b-d). Finally, automated tracking of multiple animals, simultaneously, is difficult when the animals are constantly deforming both their size and shape, however, microfluidic arenas preventing interactions of the animals greatly simplified this task.

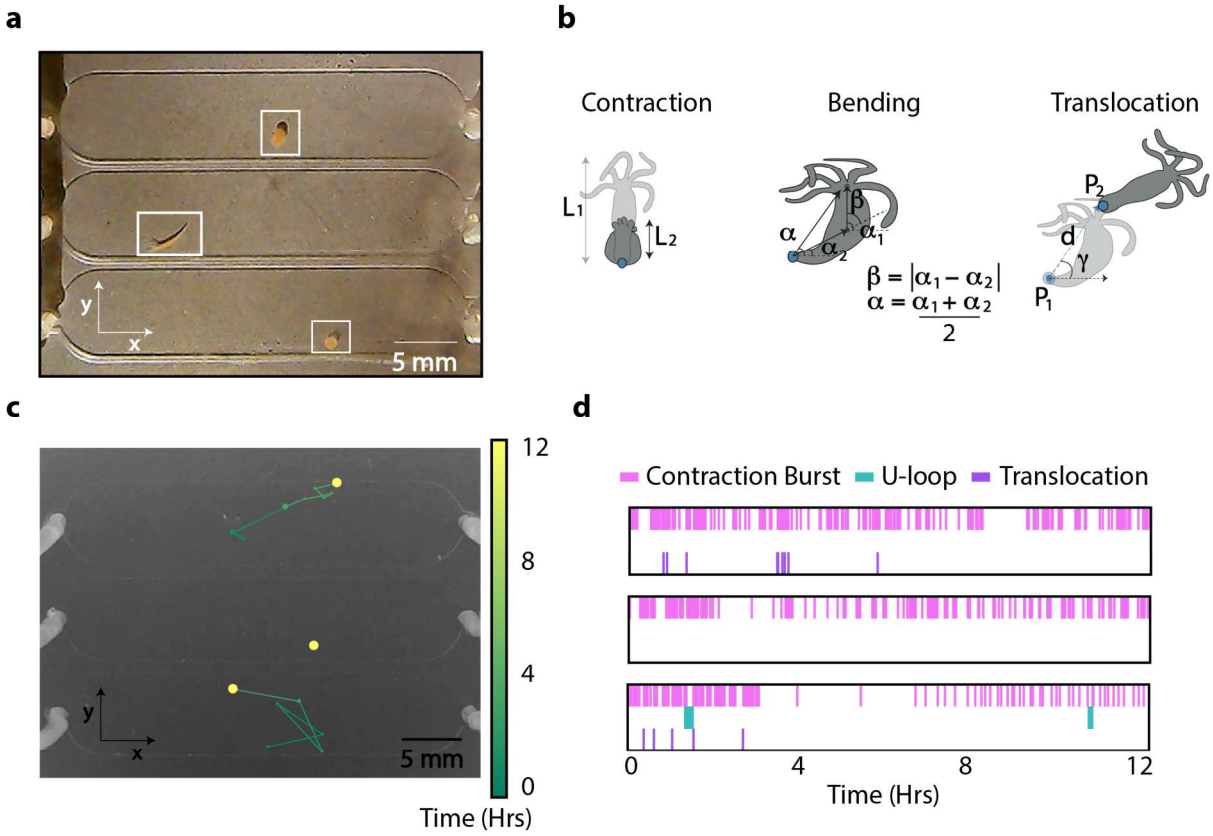

Figure 4: Behavioral Analysis in Microfluidic Arenas. (b) Photograph shows three separate microfluidic chambers for locomotion and behavioral observation of immobilized *Hydra* with uniform lighting. **(b)** Schematics show common behaviors of *Hydra* observed in microfluidic arenas: body contractions (periodic decrease in length of the body, L), exploration (reorientation of the head, α), bending (body curvature and turning head towards the foot, β), and translocation (distance and direction of displacement of the foot to new location, d and γ). **(c)** Skeletonized tracks (12 hours) of *Hydra* movements automatically tracked in the microfluidic arenas. The size of each node (dot) corresponds to the time spent at that location. The length of each edge (line) corresponds to the distance traveled during a translocation event**.** The node and edge color corresponds to the current time at that position (from start of imaging). **(d)** The raster plots indicate occurrences of each of the tracked behaviors during the 12-hour recording period.

DISCUSSION

Just as microfluidic technologies have accelerated studies of *C. elegans* and *D. melanogaster,*[22,49,51–54,58–62,71,79–81] we believe that the electrophysiology, imaging, environmental control, and behavioral tracking made possible with the microfluidic technologies shown here will help *Hydra* become a more powerful model organism. In particular, we have found that despite the soft and deformable body of *Hydra*, we can

create microfluidic chambers than can immobilize the animal with varying levels of confinement. The easy loading and unloading protocol means the same *Hydra* can be studied over several days. Moreover, the microfluidic platform allows gentle perfusion of chemicals and buffers for stimulating behaviors or studying locomotive behaviors in complex chemical, thermal, or optical landscapes.

As a demonstration of the types of experiments enabled by microfluidic immobilization, we showed simultaneous electrical recordings from muscles and optical recordings from the neurons, providing insight into the patterns of neural activity that drives body column and tentacle contraction. We see this type of combined electrophysiology and whole-brain imaging as a powerful method to study coordination between neural activity and body movements - a key step toward decoding neural activity.

The *Hydra* microfluidic platform enables chemical stimulation of behavior similar to those used to probe neural circuits in other invertebrates.[69] Although *Hydra* are highly sensitive to fluid flow, we could reduce the perfusion to sufficiently slow rates and minimize the responses of *Hydra* to this mechanical stimulus. These types of experiments may help us understand the neural circuits that process external stimuli and execute resulting motor programs.

In addition, the quasi-2D environment provided by microfluidics makes it easier to quantify the *Hydra* posture and movements and facilitates whole-brain calcium imaging. Axial scanning during optical microscopy is typically the slowest scan axis because it typically requires moving an objective lens or sample stage. Thus, confining *Hydra* to a plane less than 200 μm thick will increase the rate at which one can acquire whole-brain imaging data.

Overall, the seemingly simple cnidarian *Hydra* combined with a microfluidic interrogation platform provides many opportunities to discover how complex behaviors are implemented in dynamic networks of spiking neurons. For example, the microfluidic environments described here could be used to combine whole-brain imaging with sensory motivated behaviors like chemo-, or photo-taxis. Integrating heating elements[82] or microactuators,[83] could extend these investigations to cover thermo- or mechano- sensory

processing. Because *Hydra* survive for days in these microfluidic chips, we envision that these behavioral screens could be performed with many animals in parallel over extended periods of time. Through studies like these enabled by our microfluidic platform, it may be possible to understand simple rules governing the function of highly plastic neural circuits that may be conserved in more complex brain architectures.

MATERIALS AND METHODS

Device Fabrication

The microfluidic chips were fabricated using approximately 5 mm thick layer of polydimethylsiloxane (PDMS) (Sylgard 184) molded from SU-8 2075 (MicroChem) master mold. The microfluidic chip for electrophysiology was molded from ~110 μm thick features on the master. Note that even in clonal populations of *Hydra*, the size of animals can vary significantly from 0.5mm-15 mm. Because of the lack of stereotyped dimensions of *Hydra*, it is difficult to optimize the dimensions of the immobilization chambers to accommodate the entire population. Thus, we designed the pinch areas such that it would accommodate a subpopulation of animals. We tried 200μm-500μm width and 300-600μm length for the pinch area and found that we could select few animals that would fit optimally in any one of the dimensions. For the purpose of the experiments, we selected pinch area that accommodated animals that were just large enough to be viewed almost in entirety in the field of view (10x objective).

For the hour-glass chips, we found that chamber width of ~110μm provided a good balance between strong immobilization without causing significant damage for a range of Hydra sizes (approximately 0.5 – 2 mm in length). We found that cambers of 80-90μm in width, reduced the range of sizes of the animals that could be immobilized without causing noticeable damage. We found that about ~50% of the animals showed visible injury during immobilization in these thinner chambers. In the case of thicker chambers (up to 200μm), we rarely (<5%) observed damage, however the resulting motion that these wide

chambers permitted made it difficult to image cellular-level calcium activity as the animals were able to move more frequently.

The chemical perfusion chip was molded from a master mold fabricated with two layers, ~25 μm perfusion channels with SU-8 3025 and ~150 μm observation chamber with SU-8 2075. The behavioral microfluidic arena was fabricated from ~600 μm tall parallel channels master mold. The ports for inserting tubing were punched with either 1 or 1.5 mm biopsy punches. Larger biopsy punch was used for *Hydra* insertion port. The microfluidic chips for chemical perfusion and behavioral arena were permanently bonded to glass wafer with oxygen plasma treatment at 330 mTorr for 30 sec. The microfluidic chips for electrophysiology and imaging were clamped to the nano-SPEAR chip with a customized acrylic enclosure. Clamping with acrylic instead of permanently bonding PDMS to the electrophysiology chip makes cleaning the device easier between uses.

The electrical interrogation device is a combination of electrophysiology chip interfaced with a microfluidic chip similarly to the previously reported nano-SPEARs chip.[71] The electrophysiology device was fabricated on a glass substrate (University Wafers) using micro- and nano-fabrication techniques. A layer of KMPR photoresist was spun on the glass wafer. Platinum electrodes were patterned on the first KMPR layer. A second layer of KMPR was patterned with the immobilization chamber on top of the Pt electrodes using photolithography. The recording chambers patterned on the top KMPR layer were then etched to the bottom KMPR layer with reactive ion etcher (RIE) resulting in suspended electrodes. To increase the longevity of the device, the entire device was coated with Parylene C which acts as a water barrier. The tips of the electrodes were exposed with focused ion beam milling. KMPR has high autofluorescence which contributes to high background fluorescence during calcium imaging. A thin layer of Chromium (~ 60nm) was sputtered on glass wafer before the first KMPR layer to block excitation light from reaching photoresist. The Cr was removed from the recording chamber region after the final RIE step with wet chromium etchant (MicroChem) to allow excitation light to reach the *Hydra* in immobilization chamber. The Pt pads on the fabricated electrophysiology chip were connected to electrical leads with conductive

475 epoxy. A microfluidic chip with similar immobilization chamber pattern (Fig. 2a) was aligned on top of the
476 electrophysiology chip.
477
478 All microfluidic chips were reusable after cleaning. The microfluidic chips for electrophysiology and
479 imaging were rinsed with deionized water and oven dried at 80C for at least 40 minutes. The microfluidic
480 chips used with chemicals were soaked in deionized water overnight (at least 10 hours) on a stir plate,
481 sonicated in fresh deionized water for at least 10 minutes, heated to 160C for 1 hour, and finally oven
482 dried at 80C for at least 40 minutes before reusing. We did not observe tentacle writhing-like behavior in
483 the previously used devices (with GSH for feeding response) that were soaked in deionized water for at
484 least 8 hours.
485
486 ***Hydra* Strains and Maintenance**
487
488 The *Hydra vulgaris* AEP strains including the wild type (WT) and the two transgenic *Hydra vulgaris* lines
489 expressing either GCaMP6s in their neurons (GCAMP6s, neurons) and GFP in the neurons (GFP,
490 neurons) were provided by Christophe Dupre in the laboratory of Rafael Yuste (Columbia University). The
491 transgenic lines of *Hydra* were developed by embryo microinjection as previously reported.[48,84,85] All
492 *Hydra* were cultured in *Hydra* Media using the protocol adapted from Steele laboratory (UC Irvine). *Hydra*
493 were fed freshly hatched brine shrimp (artemia naupali) at least three times a week and the *Hydra* Media
494 was replaced approximately 1-4 hours after feeding to remove excess food. The *Hydra* culture containers
495 were thoroughly cleaned every four weeks to remove any film buildup. Individual *Hydra* were starved for
496 at least 2 days prior to experiments with the exception of experiment with glutathione induced feeding
497 behavior, where the animals were starved for at least 4 days.
498
499 ***Hydra* Loading and Unloading**
500
501 *Hydra* was inserted into the microfluidic devices through a syringe cap attached to 1 mm tygon tubing that
502 was inserted into the entry port. Using a glass pipette, *Hydra* was dropped into an open syringe cap then

using the syringe connected to the port on the opposite end of the microfluidic immobilization chamber, negative pressure was used to pull the polyp into the immobilization chamber. During this process, the open syringe cap was connected to a syringe containing *Hydra* media to prevent inserting air into the device. In case when *Hydra* adhered to the tubing, alternating positive and negative pressures helped dislodge the *Hydra*. If *Hydra* still remained stuck, gentle localized tapping dislodged the *Hydra* to resume flow. This approach required working fairly quickly once the *Hydra* was dropped into the open syringe cap to prevent undesired adhesion to the plastic surfaces. Because of this stickiness, we had approximately 50% success rate for loading *Hydra* without causing significant damage and took up to 5 minutes to load an animal that adhered to plastic surfaces. The second loading method reduced contact with plastic by pulling the *Hydra* few millimeters into the tubing with syringe then inserting the tubing into the inlet port of the microfluidic device. This approach increased success rate to 95% and took less than a minute to load an animal, though care had to be taken to not introduce any air into the microfluidic chamber. *Hydra* was loaded by applying positive pressure to the inlet syringe. The two opposing syringes were alternatively used to provide gentle pulses to position the *Hydra* at the recording site. At the end of the experimentation, *Hydra* could be removed from the microfluidic device either by disassembling the device or by gently pulsing the syringes to flow *Hydra* out of the large inlet port.

Hydra Electrophysiology

Electrophysiology chip interfaced with PDMS was clamped with acrylic and the electrical leads were connected to the amplifier. All data was obtained with an Intan Technologies RHD2132 unipolar input amplifier (http://intantech.com) at a sampling rate of 10 KHz (for electrophysiology of *H. Vulgaris* AEP animals), low frequency cutoff and DSP filter of 0.1 Hz and high frequency cutoff of 7.5 KHz.

For electrophysiological experiments, *Hydra* starved for at least 48 hours was immobilized in the recording chamber and the recording began at least 5 minutes after *Hydra* had been immobilized. The animals were recorded from under ‘dark’ conditions with ambient light passed through red filter (Red filter #26, Roscolux). Six animals were recorded for one hour each (Fig. 2 - Supplement Fig. 1) and three

animals were recorded for 10 hours each (Fig. 2). The nano-SPEARs measured bursts of electrical activity when the animal contracted. These measurements resemble contraction bursts that are known to be associated with contraction. In cases when *Hydra* drifted away from the electrodes, we noticed decrease in signal amplitude. However, we could reestablish electrical contact by applying pressure from either the entry or the suction ports to reposition the animal.

Electrophysiology data had two obvious waveforms that correspond to behaviors: small spikes during tentacle contractions, large spikes during body contractions (Fig. 2 - Supplement Fig. 1). The K-Means algorithm for clustering showed there were two optimal clusters. We manually selected spike amplitude threshold of 500 μV to derive the two distinct waveforms. In biphasic or triphasic waveforms, the largest negative or positive peak was used for the spike amplitude. Spike width was determined by calculating the full width half max (FWHM) of the waveform. Successive large amplitude contraction pulses separated by 10 s or less were considered a part of the same contraction burst and the inter-pulse interval was the time between these pulses in a single contraction burst. Inter-burst interval was the time between contraction bursts.

Simultaneous Imaging and Electrophysiology

Electrical measurements with nano-SPEARs were made while simultaneously performing brightfield or fluorescence imaging of either wild type or transgenic animal, respectively. Brightfield imaging was performed (10 fps, 60 min, 0.13 N.A. 4x objective, and 'dark' lighting (see *Hydra* Electrophysiology methods)) to record behaviors such as contractions occurring during measurement of electrical activity (Supplementary Movie 2). Transgenic *Hydra* expressing GCaMP6s in the neurons starved for at least 48 hours were used to measure the activity of the neurons (20 fps, 60 min, 0.45 N.A. 10x objective, and 20% light intensity with GFP filter) (Supplementary Movie 3). An inverted microscope equipped with GFP filter and Andor Zyla 4.2 were used for capturing all of the images. All electrical data was obtained with an Intan Technologies RHD2132 unipolar input amplifier (http://intantech.com) at a sampling rate of 1KHz

(neuronal GCaMP) or 10 KHz (WT) low frequency cutoff and DSP filter of 0.1 Hz and high frequency cutoff of 7.5 KHz.

Data shown in Fig. 2 is representative of all animals tested (N = 3, GCaMP6s positive neurons, N = 9, WT). In GCaMP animals, photobleaching limited the maximum imaging time to between 20 min (N=1) and roughly 1 hour (N=2). Movement or calcium activity correlation with electrical activity (data shown in Fig. 2c, d) was performed on animals that remained in the field of view for the entire 1 hour of electrical recording. For both WT and GCaMP animals, correlating movement or calcium activity with the entire duration of the electrical measurements was limited by animal expansion outside of the imaging field of view to roughly 30 min (N=8, WT and N=2, GCaMP6 positive neurons; representative data shown in Supplementary Fig. 3, 5) and 1 hour (N=1, WT and N=1 GCaMP; Supplementary Fig. 2, 4 and Fig. 2).

Movement Analysis for Simultaneous Electrophysiology and Imaging

Electrical activity from *Hydra* was recorded simultaneously with brightfield imaging. To track the animal movement, we looked at the change in body size (area). During body contractions, the entire body of the animal decreased in size (area). During tentacle contractions, upper half of the body containing the tentacles decreased in size (area). Thus, decrease in body size occurred during contractions. To measure the body size (area), we first binarized the images to extract *Hydra* region with Matlab Image Processing Toolbox. From the binarized image, we calculated the number of pixels forming whole *Hydra* body, upper half only or the lower half only.

During body contractions, entire body including all tentacles contracted resulting in large decrease in entire body area while during tentacles contraction, only few of the tentacles contracted resulting in smaller decrease in upper body half (hypostomal region). Thus, the change in size for the upper body half was used to generate movement trace (Fig 2c).

To generate the movement map (Fig. 2c, bottom right image in each box), we overlaid the binarized images of the *Hydra* and used the color map to represent the fraction of the time that the *Hydra* occupied each pixel. Thus, the light-colored areas of the map show the locations of body and tentacle contractions. Because *Hydra* remains contracted longer during closely occurring contraction bursts, dark-colored area of the map shows *Hydra* in its most contracted form (Fig, 2c left box). We used a 150 s time window to show body contractions more clearly because contraction bursts can last more than 30 s and sometimes animals do not elongate significantly between bursts. For correlation of tentacle contractions, we used a 30 s time window, which is comparable to the time scale of tentacle contractions.

Correlation Analysis for Simultaneous Electrophysiology and Imaging

To determine the correlation significance, we first normalized the electrical measurements and movement (for WT movement correlation analysis) or calcium activity (for neural GCaMP calcium activity correlation analysis) measurements. We then segmented the time series for each set of data into 30 s intervals. By sliding a 30 s time window across the entire recording by 5 s, we generated a set of approximately 714 (30-second-long) recording intervals. We then computed cross-correlation values between electrical measurements and movement (or calcium activity) for each time-aligned interval. We then grouped these cross-correlation values based on whether the time interval contained “high” (> 0.3 a.u.) or “low” (< 0.3 a.u.) electrical activity and plotted those distributions in Supplementary Fig. 2-5b. To determine if these cross-correlation values were statistically significant, we computed the cross-correlation values after randomizing the time intervals (shuffling the time series). We found that 99% of correlation values in the shuffled data were below 315 a.u. (WT) or 10 a.u. (neural GCaMP), which we used as the thresholds for statistical significance (dashed line in Supplementary Fig. 2-5b). We found that the mean correlation value exceeded the threshold for statistical significance during periods of high electrical activity (Supplementary Fig. 2-5b).

Normalization for the electrical measurements involved taking the absolute value of the electrical activity to account both the positive and negative spikes (Supplementary Fig. 2-5a top). Then, we applied a Gaussian low pass filter and down-sampled the data to 100Hz to smooth the electrical measurements and finally, rescaled the range to be between 0 and 1. The normalized electrical measurements were then split into 30 s time intervals. Multiple intervals (714) were generated by sliding across the entire recording period by 5 seconds. Each of the intervals were grouped as high or low activity periods based on whether the interval contained high or low amplitude activity (threshold of 0.3 a.u. was used).

Similarly, the movement (Supplementary Fig. 2,3a) and calcium activity (Supplementary Fig. 4,5a) measurements were first normalized then segmented into 30 s intervals. For movement analysis, the data were number of pixels comprising the entire body, upper body or lower body. Because body contractions led to decrease in body size, the raw movement data were first inverted such that the values would increase during body contractions. We then applied a Gaussian low pass filter, up-sampled to 100Hz and rescaled the range to be between 0 and 1. For neural activity analysis, the data were average of relative fluorescence values of all pixels for the entire body, upper body or lower body. The fluorescence traces were normalized by first calculating the $\Delta F/F$ to correct baseline drift due to photobleaching. Then we applied a Gaussian low pass filter, up-sampled to 100Hz and rescaled the range to be between 0 and 1. Finally, we segmented the movement and calcium imaging activity traces into 30 s intervals. By sliding the interval by 5 s, we generated 714 intervals that were time-aligned with the intervals for electrical measurements. Each of the time intervals were grouped as high or low activity periods depending on whether their time-aligned electrical measurement intervals were high or low activity periods.

Maximum value of correlogram from the time-aligned (unshuffled) intervals was computed to determine average correlation during high and low activity periods for the entire body and upper and lower body segments for both movement (Supplementary Fig. 2,3b) and neural activity analysis (Supplementary Fig 4,5b.). Both the Intan amplifier and the Zyla were triggered with the same TTL signal. However, to account for any offset in the timing of the electrical and optical data, we measured the maximum of the cross-correlogram within one duty cycle of the trigger signal (50 ms) rather than the cross-correlation at

zero lag. To determine statistical significance of the correlation values, maximum value of correlogram was computed for the 714 intervals that were randomly selected (shuffled) for each animal such that electrical measurement intervals were no longer time-aligned with movement or neural activity intervals. From the distribution of shuffled correlation values, we set the significance threshold to include 99% of the correlation values from the shuffled data. Correlation values outside this 99% confidence interval were considered significant. From our WT movement correlation analysis, we found 99% of the correlation values were below 315 a.u. with 30 s intervals and high activity periods had statistically significant correlation. For our neural GCaMP calcium activity correlation analysis, we found 99% of the correlation values were below 10 a.u. with 30 s intervals and high activity periods had statistically significant correlation.

Because tracking individual neurons purely from fluorescence from calcium indicator in deforming *Hydra* is difficult, we commuted spatially-resolved cross-correlation of representative 30 s interval from high activity period and low activity period. This allowed us to identify regions in *Hydra* body that had correlated neural activity with electrical activity during a 30 s high activity or low activity period. The high and low amplitude activity regions were identified with threshold as discussed above (Fig, 2c, d). The high amplitude activity region occurred during contraction bursts for neural activity imaging. The low amplitude activity region occurred during rhythmic potential like activity during neural imaging. For the spatially-resolved correlation maps (Fig 2 d), each frame was down-sampled to 64 x 64 pixels and the vectors of fluorescence values for each of the down-sampled pixels were normalized for the full recording period by applying a Gaussian low pass filter, up-sampling to 100Hz then rescaling the range for the entire image (all 64x 64 pixels) to be from 0 to 1 preserving the relative intensity differences between individual pixels (and reduce contribution from background fluctuations due to light scattering). The correlation value from each of the pixels was then used to determine the intensity of the pixel for the correlation map. The pixel intensity was mapped to a color map that represented pixels with correlation values below statistical significance threshold (determined from the shuffled data as discussed above) as white color. Above the threshold for statistically significant correlation values, the pixel colors ranged from blue to yellow (with yellow corresponding to higher correlation values than blue). Note that the background pixels in the hour-

glass chamber not overlapping the *Hydra* body show statistically significant correlation values (blue color) due to scattering of fluorescence from nearby regions during body contractions. This scattering could be reduced with higher contrast laser scanning imaging such as confocal imaging. Nonetheless, the correlation values for background pixels were found to be lower than correlation values for pixels that were inhabited by *Hydra* and more specifically the pixels encompassing the *Hydra* foot. Thus, short of tracking individual neurons, which is difficult in *Hydra*, the spatially-resolved correlation map allowed us to correlate activity from clusters of neurons with electrical activity.

Imaging for Micro-Movement Analysis

WT Hydra (*H. Vulgaris* AEP) was placed in a petri dish and imaged on our behavioral imaging platform to estimate the movement without microfluidic confinement. Images were captured for 15 minutes at ~8fps. The position of the foot and the mouth were annotated using the foot and mouth classification algorithm from our behavior and locomotion tracking algorithm (see methods, Behavior and Locomotion Tracking). Microscope image calibration ruler was used to estimate the pixel size. Frame to frame movement of the foot (286 μm/min) and mouth (266 μm/min) was calculated to estimate the movement.

Transgenic *Hydra* expressing GCaMP6s in the neurons was immobilized in an electrophysiology chip to estimate the movement after microfluidic immobilization. *Hydra* movement was imaged with 488nm excitation laser and 0.45 N.A. 10x objective on Nikon Ti Eclipse Confocal microscope for 5 minutes at ~1 fps. Few cells with constant fluorescence were tracked for motion to calculate displacement and average movement of cells (65 μm/minute) in the body column of *Hydra* immobilized in hour-glass chambers.

Chemical Stimulation with Reduced Glutathione for Feeding Response

Hydra (*H. Vulgaris* AEP) were starved for at least 4 days prior to immobilization in the perfusion chambers for chemical stimulation. One side of the port connecting to the perfusion channels was used as the perfusion inlet port. Two syringes with stopcock valves containing either *Hydra* media or 9μM reduced glutathione (GSH) (Biosynth) were connected to a 2 to 1 manifold which was then connected to the perfusion inlet port. The inlet syringes were raised ~25 cm above the device to hydrostatically flow chemicals/buffer. Opposite side of the perfusion channels used as the outlet were connected to a syringe at the same height as the device. To calculate the flow rates into the observation chamber, we ignored all fluidic paths except narrow perfusion channels because the fluidic resistance in the narrow perfusion channels was significantly higher than in the tubing and thus had the largest contribution to flow rates. This calculation was in agreement with the approximately 0.02 mL/min change in syringe volume we observed during the experiments. After immobilization of the *Hydra*, different flow conditions were used while imaging behavioral changes for 30 minutes each. First, 30 minutes of baseline activity was imaged with no flow, followed by 30 minutes with flow of *Hydra* media to show minimal effects of slow perfusion on *Hydra* behavior. Next, perfusion input was switched to GSH for 30 minutes to cause the mouth to open and to inhibit body contractions. We began to measure response roughly 20 minutes after beginning the flow of GSH. Finally, the perfusion input was switched again to *Hydra* media for 30 minutes to terminate feeding response and recover normal contractile activity (Supplementary Movie 4). All brightfield imaging during chemical stimulation was performed using 0.13 N.A. 4x objective and Zyla4.2 at ~5 fps for 2 hours in 3 mm wide and ~160 μm tall observation chamber.

To obtain the *Hydra* length trace (Fig. 3c), we created binary images of the *Hydra* and used the major axis length from binary region properties using Matlab Image Processing Toolbox. During body contractions, body length decreases significantly as the *Hydra* contracts into a tight ball. The body length increases when the animal elongates. As a result, the traces of body length show large fluctuations indicating spontaneous body contractions for the first half of the experiment (60 minutes) and more constant body length once stimulated with GSH and mouth begins to open. The fluctuations in body length begin to return following wash with buffer. If the experiment is allowed to continue with wash buffer

for another 30 minutes, the body contraction rate begins to approach the contraction rate prior to stimulation.

Transgenic Hydra (GCaMP6s, neurons) was starved for at least 4 days prior to immobilization and chemical stimulation. Fluorescence imaging during chemical stimulation was performed using 0.45 N.A. 10x objective, 12% epifluorescence light intensity and Zyla4.2 at ~15 fps for 1 hour in 3 mm wide and ~160 μm tall observation chamber. Because effective imaging time with fluorescence calcium indicator was close to thirty minutes before photobleaching occurred, the flow conditions were modified to reduce exposure to excitation light before chemical stimulation. First, the period of baseline activity measurement without flow was eliminated and period of *Hydra* media flow was reduced to five minutes. This was followed with GSH flow for thirty minutes, and finally recovery with *Hydra* media for thirty minutes (Supplementary Movie 5).

Chemical Stimulation with Chloretone for Muscle Paralysis

Transgenic *Hydra* expressing GFP in the neurons was immobilized in the ~160 μm tall perfusion chambers for stimulation with 0.1% Chloretone (Acros Organics). The *Hydra* was imaged using 488nm excitation laser and 0.45 NA 10x objective and ~1fps on Nikon Ti Eclipse Confocal for tracking the neurons before and after being anesthetized. After perfusion of Chloretone, the animal movement was significantly decreased and the whole-brain anatomy was volumetrically imaged at high resolution with negligible motion artifacts (Fig. 1b).

Behavior and Locomotion Tracking

Hydra (H. vulgaris AEP) raised in dark at 20C and fed three times a week under ambient light were used for behavioral and locomotive tracking. Time-lapse imaging was performed using portable USB digital microscope/mini microscope endoscope (TOPMYS TM-M200, www.amazon.com). Images were captured at a rate of 1 frame every second on open-source camera software iSpy (www.ispyconnect.com).

Evenly spaced 30 soft white LEDs (~ 0.8mW/cm^2) were placed below a Roscolux diffuser for evenly illuminating behavioral micro-arena from the bottom.

For behavioral tracking, *Hydra* were immobilized 2 days post feeding and imaged at 1 fps for ~60 hours at room temperature in roughly 600 μm tall microfluidic device with three 7mm wide chambers. The animals were starved for the duration of the experiment following immobilization. *Hydra* were detected using the Image Processing Toolbox in Matlab. More specifically, images were processed by background subtraction and manually adjusted threshold for binarization. Initial positions of the *Hydra* were manually provided to guide region detection. Matlab Image Processing Toolbox was used to obtain features from bianarized *Hydra* that included two endpoints and region centroid. Because *Hydra* moves relatively infrequently with foot adhering to surfaces, foot position was assigned with the endpoint that had the least movement from foot position at the previous time point (foot assignment was manually provided for the first frame). The Euclidean distances between the foot and the mouth were used to calculate the body length, L. The contraction bursts were identified as the minima in the body length values. Due to low frame rate, individual contraction burst pulses may not be sampled. To avoid counting multiple pulses within the same burst, minima with specified prominence were identified for contraction bursts. The threshold for minima was determined from the average length of the *Hydra*. The angle of the vector from the foot to the mouth with respect to the positive x-axis was used to measure the body orientation, α, for exploration. The body curvature, β, was derived from the difference in angle between vector from center of the body to the mouth, α_1, and the vector from foot to the center of the body, α_2. Small β ($\beta < \pi/3$) indicated slight bend in the body while larger β ($\pi/3 < \beta < \pi$) indicated u-loop in the body posture. A translocation event was defined by displacement in foot position above a threshold with minimum time between such displacement events. The distance, d, and the direction, γ (with respect to positive x-axis), the *Hydra* moved was calculated from a vector from the previous position to new position of *Hydra* foot. Track of locomotion pattern was overlaid on the micrograph of *Hydra* in the microfluidic arena where the size of the nodes indicated the length of stationary periods and the length of the edges connecting the two nodes indicated displacement during translocation, d (number of pixels). The color map reflects the time from start of imaging where green is the start point (0 hours) and yellow is the end point (12 hours)

778 (Fig. 4c). Raster plot of behavioral patterns was generated using above measurements (Fig 4d,
779 Supplementary Fig. 6).
780
781 To determine the frequency of translocation and contraction events, we compiled a histogram for the time
782 intervals between successive events. To confirm that translocation events were less frequent than
783 contractions, we performed one-sided, unpaired two-sample student's t-test with unequal variances (p-
784 value = 0.01, 12 hours). We performed the same statistical test (p-value = 0.005, 60 hours) on the full
785 sixty hours of recording from which the first twelve hours of data is shown in detail and found the
786 translocations events to significantly less frequent than contractions.
787
788 All analysis was performed using MATLAB (MathWorks).
789
790 **CONTRIBUTIONS**
791
792 K.N.B. performed and analyzed experiments. K.N.B. developed the microfluidic platform for *Hydra*.
793 D.L.G., K.N.B. and D.G.V. developed the fabrication process for the nano-SPEAR electrophysiology chip.
794 B.W.A. provided hardware and software support. J.T.R. directed the research. K.N.B. and J.T.R. co-wrote
795 the paper. All authors read and commented on the manuscript.
796
797
798 **ACKNOWLEDGEMENTS**
799
800 We thank Celina Juliano (UC Davis) and Stefan Siebert (UC Davis) for thoughtful discussions of *Hydra*
801 neurobiology and behaviors. We would like to thank Christophe Dupre, Dr. Rafael Yuste (Columbia
802 University), Dr. Rob Steele (UC Irvine) and Kristine Glauber for the transgenic *Hydra* strains. This work is
803 funded by the Defense Advanced Research Projects Agency Young Faculty Award D14AP00049 (J.T.R.),
804 and the DARPA BioControl program (J.T.R). K.N.B. and D.L.G. are funded by training fellowships from
805 the Keck Center of the Gulf Coast Consortia on the NSF Integrative Graduate Education and Research

Traineeship (IGERT): Neuroengineering from Cells to Systems 1250104. D.L.G is funded by the NSF Graduate Research Fellowship Program 0940902. We also thank the Rice Shared Equipment Authority and the Nanofabrication Facility where the devices were fabricated.

REFERENCES:

1 R. Bhandari, S. Negi and F. Solzbacher, Wafer-scale fabrication of penetrating neural microelectrode arrays, *Biomed. Microdevices*, 2010, **12**, 797–807.

2 J. Viventi, D.-H. Kim, L. Vigeland, E. S. Frechette, J. A. Blanco, Y.-S. Kim, A. E. Avrin, V. R. Tiruvadi, S.-W. Hwang, A. C. Vanleer, D. F. Wulsin, K. Davis, C. E. Gelber, L. Palmer, J. Van der Spiegel, J. Wu, J. Xiao, Y. Huang, D. Contreras, J. A. Rogers and B. Litt, Flexible, foldable, actively multiplexed, high-density electrode array for mapping brain activity in vivo, *Nat Neurosci*, 2011, **14**, 1599–1605.

3 D. A. Schwarz, M. A. Lebedev, T. L. Hanson, D. F. Dimitrov, G. Lehew, J. Meloy, S. Rajangam, V. Subramanian, P. J. Ifft, Z. Li, A. Ramakrishnan, A. Tate, K. Z. Zhuang and M. A. L. Nicolelis, Chronic, wireless recordings of large-scale brain activity in freely moving rhesus monkeys, *Nat Meth*, 2014, **11**, 670–676.

4 D. Khodagholy, J. N. Gelinas, T. Thesen, W. Doyle, O. Devinsky, G. G. Malliaras and G. Buzsaki, NeuroGrid: recording action potentials from the surface of the brain, *Nat Neurosci*, 2015, **18**, 310–315.

5 C. Xie, J. Liu, T.-M. Fu, X. Dai, W. Zhou and C. M. Lieber, Three-dimensional macroporous nanoelectronic networks as minimally invasive brain probes, *Nat Mater*, 2015, **14**, 1286–1292.

6 V. Emiliani, A. E. Cohen, K. Deisseroth and M. Häusser, All-Optical Interrogation of Neural Circuits, *J. Neurosci.*, 2015, **35**, 13917 LP-13926.

7 E. F. Chang, Towards Large-Scale, Human-Based, Mesoscopic Neurotechnologies, *Neuron*, 2015, **86**, 68–78.

8 M. B. Ahrens, M. B. Orger, D. N. Robson, J. M. Li and P. J. Keller, Whole-brain functional imaging at cellular resolution using light-sheet microscopy, *Nat Meth*, 2013, **10**, 413–420.

9 T.-W. Chen, T. J. Wardill, Y. Sun, S. R. Pulver, S. L. Renninger, A. Baohan, E. R. Schreiter, R. A. Kerr, M. B. Orger, V. Jayaraman, L. L. Looger, K. Svoboda and D. S. Kim, Ultra-sensitive fluorescent proteins for imaging neuronal activity, *Nature*, 2013, **499**, 295–300.

10 C. Grienberger and A. Konnerth, Imaging Calcium in Neurons, *Neuron*, 2012, **73**, 862–885.

11 R. Prevedel, Y.-G. Yoon, M. Hoffmann, N. Pak, G. Wetzstein, S. Kato, T. Schrödel, R. Raskar, M. Zimmer, E. S. Boyden and A. Vaziri, Simultaneous whole-animal 3D imaging of neuronal activity using light-field microscopy, *Nat. Methods*, 2014, **11**, 727–730.

12 T.-M. Fu, G. Hong, R. D. Viveros, T. Zhou and C. M. Lieber, Highly scalable multichannel mesh electronics for stable chronic brain electrophysiology, *Proc. Natl. Acad. Sci.*, 2017, 201717695.

13 J. J. Jun, N. A. Steinmetz, J. H. Siegle, D. J. Denman, M. Bauza, B. Barbarits, A. K. Lee, C. A. Anastassiou, A. Andrei, Ç. Aydin, M. Barbic, T. J. Blanche, V. Bonin, J. Couto, B. Dutta, S. L. Gratiy, D. A. Gutnisky, M. Häusser, B. Karsh, P. Ledochowitsch, C. M. Lopez, C. Mitelut, S. Musa, M. Okun, M. Pachitariu, J. Putzeys, P. D. Rich, C. Rossant, W. L. Sun, K. Svoboda, M. Carandini, K. D. Harris, C. Koch, J. O'Keefe and T. D. Harris, Fully integrated silicon probes for high-density recording of neural activity, *Nature*, 2017, **551**, 232–236.

14 T. H. Kim, Y. Zhang, J. Lecoq, J. C. Jung, J. Li, H. Zeng, C. M. Niell and M. J. Schnitzer, Long-Term Optical Access to an Estimated One Million Neurons in the Live Mouse Cortex, *Cell Rep.*, 2016, **17**, 3385–3394.

15 W. Zong, R. Wu, M. Li, Y. Hu, Y. Li, J. Li, H. Rong, H. Wu, Y. Xu, Y. Lu, H. Jia, M. Fan, Z. Zhou, Y. Zhang, A. Wang, L. Chen and H. Cheng, Fast high-resolution miniature two-photon microscopy for brain imaging in freely behaving mice, *Nat. Methods*, 2017, **14**, 713–719.

16 V. Venkatachalam, N. Ji, X. Wang, C. Clark, J. K. Mitchell, M. Klein, C. J. Tabone, J. Florman, H. Ji, J. Greenwood, A. D. Chisholm, J. Srinivasan, M. Alkema, M. Zhen and A. D. T. Samuel, Pan-neuronal imaging in roaming Caenorhabditis elegans, *Proc. Natl. Acad. Sci.* , 2016, **113**, E1082–E1088.

17 J. P. Nguyen, F. B. Shipley, A. N. Linder, G. S. Plummer, M. Liu, S. U. Setru, J. W. Shaevitz and A. M. Leifer, Whole-brain calcium imaging with cellular resolution in freely behaving Caenorhabditis elegans, *Proc. Natl. Acad. Sci.* , 2016, **113**, E1074–E1081.

18 D. Grover, T. Katsuki and R. J. Greenspan, Flyception: imaging brain activity in freely walking fruit flies, *Nat Meth*, 2016, **13**, 569–572.

19 W. C. Lemon, S. R. Pulver, B. Höckendorf, K. McDole, K. Branson, J. Freeman and P. J. Keller, Whole-central nervous system functional imaging in larval Drosophila, 2015, **6**, 7924.

20 M. Chalfie, J. E. Sulston, J. G. White, E. Southgate, J. N. Thomson and S. Brenner, The neural circuit for touch sensitivity in Caenorhabditis elegans, *J. Neurosci.*, 1985, **5**, 956 LP-964.

21 J. M. Gray, J. J. Hill and C. I. Bargmann, A circuit for navigation in Caenorhabditis elegans, *Proc. Natl. Acad. Sci. United States Am.* , 2005, **102**, 3184–3191.

22 K. Chung and H. Lu, Automated high-throughput cell microsurgery on-chip, *Lab Chip*, 2009, **9**, 2764–2766.

23 G. S. B. Suh, A. M. Wong, A. C. Hergarden, J. W. Wang, A. F. Simon, S. Benzer, R. Axel and D. J. Anderson, A single population of olfactory sensory neurons mediates an innate avoidance behaviour in Drosophila, *Nature*, 2004, **431**, 854–859.

24 J. Y. Yu, M. I. Kanai, E. Demir, G. S. X. E. Jefferis and B. J. Dickson, Cellular Organization of the Neural Circuit that Drives Drosophila Courtship Behavior, *Curr. Biol.*, 2010, **20**, 1602–1614.

25 L. Avery and H. R. Horvitzt, Pharyngeal pumping continues after laser killing of the pharyngeal nervous system of C. elegans, *Neuron*, 1989, **3**, 473–485.

26 C. I. Bargmann and H. R. Horvitz, Chemosensory neurons with overlapping functions direct chemotaxis to multiple chemicals in C. elegans, *Neuron*, 1991, **7**, 729–742.

27 C. I. Bargmann, E. Hartwieg and H. R. Horvitz, Odorant-selective genes and neurons mediate olfaction in C. elegans, *Cell*, 1993, **74**, 515–527.

28 C. I. Bargmann and L. Avery, Laser Killing of Cells in Caenorhabditis elegans, *Methods Cell Biol.*, 1995, **48**, 225–250.

29 S. H. Chalasani, N. Chronis, M. Tsunozaki, J. M. Gray, D. Ramot, M. B. Goodman and C. I. Bargmann, Dissecting a circuit for olfactory behaviour in Caenorhabditis elegans, *Nature*, 2007, **450**, 63–70.

30 A. Kuhara, M. Okumura, T. Kimata, Y. Tanizawa, R. Takano, K. D. Kimura, H. Inada, K. Matsumoto and I. Mori, Temperature Sensing by an Olfactory Neuron in a Circuit Controlling Behavior of C. elegans, *Science (80-.).*, 2008, **320**, 803 LP-807.

31 E. Fishilevich, A. I. Domingos, K. Asahina, F. Naef, L. B. Vosshall and M. Louis, Chemotaxis Behavior Mediated by Single Larval Olfactory Neurons in Drosophila, *Curr. Biol.*, 2005, **15**, 2086–2096.

32 R. J. Nudo, E. J. Plautz and S. B. Frost, Role of adaptive plasticity in recovery of function after damage to motor cortex, *Muscle Nerve*, 2001, **24**, 1000–1019.

33 G. li Ming and H. Song, Adult Neurogenesis in the Mammalian Brain: Significant Answers and Significant Questions, *Neuron*, 2011, **70**, 687–702.

34 T. H. Murphy and D. Corbett, Plasticity during stroke recovery: from synapse to behaviour, *Nat. Rev. Neurosci.*, 2009, **10**, 861–872.

35 A. Gierer, S. Berking, H. Bode, C. N. David, K. Flick, G. Hansmann, C. H. Schaller and E. Trenkner, *Nature/New Biol.*, 1972, 98–101.

36 U. Technau, C. Cramer von Laue, F. Rentzsch, S. Luft, B. Hobmayer, H. R. Bode and T. W. Holstein, Parameters of self-organization in Hydra aggregates, *Proc. Natl. Acad. Sci.*, 2000, **97**, 12127 LP-12131.

37 S. Ghosh-dastidar and A. G. Lichtenstein, Review Article SPIKING NEURAL NETWORKS, 2009, **19**, 295–308.

38 J. A. Chapman, E. F. Kirkness, O. Simakov, S. E. Hampson, T. Mitros, T. Weinmaier, T. Rattei, P. G. Balasubramanian, J. Borman, D. Busam, K. Disbennett, C. Pfannkoch, N. Sumin, G. G. Sutton, L. D. Viswanathan, B. Walenz, D. M. Goodstein, U. Hellsten, T. Kawashima, S. E. Prochnik, N. H. Putnam, S. Shu, B. Blumberg, C. E. Dana, L. Gee, D. F. Kibler, L. Law, D. Lindgens, D. E. Martinez, J. Peng, P. A. Wigge, B. Bertulat, C. Guder, Y. Nakamura, S. Ozbek, H. Watanabe, K. Khalturin, G. Hemmrich, A. Franke, R. Augustin, S. Fraune, E. Hayakawa, S. Hayakawa, M. Hirose, J. S. Hwang, K. Ikeo, C. Nishimiya-Fujisawa, A. Ogura, T. Takahashi, P. R. H. Steinmetz, X. Zhang, R. Aufschnaiter, M.-K. Eder, A.-K. Gorny, W. Salvenmoser, A. M. Heimberg, B. M. Wheeler, K. J. Peterson, A. Bottger, P. Tischler, A. Wolf, T. Gojobori, K. A. Remington, R. L. Strausberg, J. C. Venter, U. Technau, B. Hobmayer, T. C. G. Bosch, T. W. Holstein, T. Fujisawa, H. R. Bode, C. N. David, D. S. Rokhsar and R. E. Steele, The dynamic genome of Hydra, *Nature*, 2010, **464**, 592–596.

39 H. Watanabe, T. Fujisawa and T. W. Holstein, Cnidarians and the evolutionary origin of the nervous system, *Dev. Growth Differ.*, 2009, **51**, 167–183.

40 T. C. G. Bosch, A. Klimovich, T. Domazet-Loš, S. Gründer, T. W. Holstein, G. Jékely, D. J. Miller,

924 A. P. Murillo-Rincon, F. Rentzsch, G. S. Richards, K. Schröder, U. Technau and R. Yuste, Back to
925 the Basics: Cnidarians Start to Fire, *Trends Neurosci.*, 2016, **xx**, 1–14.
926 41 J. A. Westfall, J. C. Kinnamon and D. E. Sims, Neuro-epitheliomuscular cell and neuro-neuronal
927 gap junctions inHydra, *J. Neurocytol.*, 1980, **9**, 725–732.
928 42 J. C. Kinnamon and J. a Westfall, Types of neurons and synaptic connections at hypostome-
929 tentacle junctions in Hydra., *J. Morphol.*, 1982, **173**, 119–28.
930 43 S. Gründer and M. Assmann, Peptide-gated ion channels and the simple nervous system of
931 Hydra, *J. Exp. Biol.*, 2015, **218**, 551 LP-561.
932 44 J. A. Westfall, S. Yamataka and P. D. Enos, Ultrastructural evidence of polarized synapses in the
933 nerve net of hydra, *J. Cell Biol.*, 1971, **51**, 318–323.
934 45 J. A. Westfall, Ultrastructural evidence for a granule-containing sensory-motor-interneuron in
935 Hydra littoralis, *J. Ultrastruct. Res.*, 1973, **42**, 268–282.
936 46 L. E. Davis, A. L. Burnett, J. F. Haynes, D. G. Osborne and M. Lou Spear, Histological and
937 ultrastructural study of the muscular and nervous systems in Hydra. II. Nervous system, *J. Exp.*
938 *Zool.*, 1968, **167**, 295–331.
939 47 J. P. Dexter, M. B. Tamme, C. H. Lind and E.-M. S. Collins, On-chip immobilization of planarians
940 for in vivo imaging., *Sci. Rep.*, 2014, **4**, 6388.
941 48 C. Dupre and R. Yuste, Non-overlapping Neural Networks in Hydra vulgaris, *Curr. Biol.*, 2017, **27**,
942 1085–1097.
943 49 M. M. Crane, K. Chung, J. Stirman and H. Lu, Microfluidics-enabled phenotyping, imaging, and
944 screening of multicellular organisms, *Lab Chip*, 2010, **10**, 1509–1517.
945 50 M. F. Yanik, C. B. Rohde and C. Pardo-Martin, Technologies for Micromanipulating, Imaging, and
946 Phenotyping Small Invertebrates and Vertebrates, *Annu. Rev. Biomed. Eng.*, 2011, **13**, 185–217.
947 51 H. Hwang and H. Lu, Microfluidic tools for developmental studies of small model organisms —
948 nematodes, fruit flies, and zebrafish, *Biotechnol. J.*, 2013, **8**, 192–205.
949 52 T. J. Levario, M. Zhan, B. Lim, S. Y. Shvartsman and H. Lu, Microfluidic trap array for massively
950 parallel imaging of Drosophila embryos, *Nat. Protoc.*, 2013, **8**, 721–736.
951 53 K. Chung, Y. Kim, J. S. Kanodia, E. Gong, S. Y. Shvartsman and H. Lu, A microfluidic array for

large-scale ordering and orientation of embryos, *Nat Meth*, 2011, **8**, 171–176.

54 E. M. Lucchetta, J. H. Lee, L. A. Fu, N. H. Patel and R. F. Ismagilov, Dynamics of Drosophila embryonic patterning network perturbed in space and time using microfluidics, *Nature*, 2005, **434**, 1134–1138.

55 T. J. Levario, B. Lim, S. Y. Shvartsman and H. Lu, Microfluidics for High-Throughput Quantitative Studies of Early Development, *Annu. Rev. Biomed. Eng.*, 2016, **18**, 285–309.

56 T. J. Levario, C. Zhao, T. Rouse, S. Y. Shvartsman and H. Lu, An integrated platform for large-scale data collection and precise perturbation of live Drosophila embryos, *Sci. Rep.*, 2016, **6**, 21366.

57 F. Zeng, C. B Rohde and M. Yanik, *Sub-cellular precision on-chip small-animal immobilization, multi-photon imaging and femtosecond-laser manipulation*, 2008, vol. 8.

58 S. E. Hulme, S. S. Shevkoplyas, J. Apfeld, W. Fontana and G. M. Whitesides, A microfabricated array of clamps for immobilizing and imaging C. elegans, *Lab Chip*, 2007, **7**, 1515–1523.

59 C. B. Rohde, F. Zeng, R. Gonzalez-Rubio, M. Angel and M. F. Yanik, Microfluidic system for on-chip high-throughput whole-animal sorting and screening at subcellular resolution, *Proc. Natl. Acad. Sci.* , 2007, **104**, 13891–13895.

60 K. Chung, M. M. Crane and H. Lu, Automated on-chip rapid microscopy, phenotyping and sorting of C. elegans, *Nat Meth*, 2008, **5**, 637–643.

61 S. R. Lockery, K. J. Lawton, J. C. Doll, S. Faumont, S. M. Coulthard, T. R. Thiele, N. Chronis, K. E. McCormick, M. B. Goodman and B. L. Pruitt, Artificial Dirt: Microfluidic Substrates for Nematode Neurobiology and Behavior, *J. Neurophysiol.*, 2008, **99**, 3136 LP-3143.

62 C. L. Gilleland, C. B. Rohde, F. Zeng and M. F. Yanik, Microfluidic immobilization of physiologically active Caenorhabditis elegans., *Nat. Protoc.*, 2010, **5**, 1888–1902.

63 N. Chronis, Worm chips: Microtools for C. elegans biology, *Lab Chip*, 2010, **10**, 432–437.

64 J. N. Stirman, M. Brauner, A. Gottschalk and H. Lu, High-throughput study of synaptic transmission at the neuromuscular junction enabled by optogenetics and microfluidics, *J. Neurosci. Methods*, 2010, **191**, 90–93.

65 K. E. McCormick, B. E. Gaertner, M. Sottile, P. C. Phillips and S. R. Lockery, Microfluidic Devices

for Analysis of Spatial Orientation Behaviors in Semi-Restrained Caenorhabditis elegans, *PLoS One*, 2011, **6**, e25710.

66 M. M. Crane, J. N. Stirman, C.-Y. Ou, P. T. Kurshan, J. M. Rehg, K. Shen and H. Lu, Autonomous screening of C. elegans identifies genes implicated in synaptogenesis, *Nat. Methods*, 2012, **9**, 977.

67 B. M. Song, S. Faumont, S. Lockery and L. Avery, Recognition of familiar food activates feeding via an endocrine serotonin signal in Caenorhabditis elegans, *Elife*, 2013, **2013**, 1–27.

68 N. Chronis, M. Zimmer and C. I. Bargmann, Microfluidics for in vivo imaging of neuronal and behavioral activity in Caenorhabditis elegans, *Nat Meth*, 2007, **4**, 727–731.

69 D. R. Albrecht and C. I. Bargmann, High-content behavioral analysis of Caenorhabditis elegans in precise spatiotemporal chemical environments, *Nat Meth*, 2011, **8**, 599–605.

70 S. R. Lockery, S. E. Hulme, W. M. Roberts, K. J. Robinson, A. Laromaine, T. H. Lindsay, G. M. Whitesides and J. C. Weeks, A microfluidic device for whole-animal drug screening using electrophysiological measures in the nematode C. elegans, *Lab Chip*, 2012, **12**, 2211–2220.

71 D. L. Gonzales, K. N. Badhiwala, D. G. Vercosa, B. W. Avants, Z. Liu, W. Zhong and J. T. Robinson, Scalable electrophysiology in intact small animals with nanoscale suspended electrode arrays, *Nat Nano*.

72 J. A. Carter, C. Hyland, R. E. Steele and E.-M. S. Collins, Dynamics of Mouth Opening in Hydra, *Biophys. J.*, 2016, **110**, 1191–1201.

73 U. Technau and R. E. Steele, Evolutionary crossroads in developmental biology: Cnidaria, *Development*, 2011, **138**, 1447 LP-1458.

74 P. J. Hung, P. J. Lee, P. Sabounchi, R. Lin and L. P. Lee, Continuous perfusion microfluidic cell culture array for high-throughput cell-based assays, *Biotechnol. Bioeng.*, 2005, **89**, 1–8.

75 W. Grosvenor, D. E. Rhoads and G. Kass-Simon, Chemoreceptive control of feeding processes in hydra, *Chem. Senses*, 1996, **21**, 313–321.

76 S. Han, E. Taralova, C. Dupre and R. Yuste, Comprehensive machine learning analysis of Hydra behavior reveals a stable behavioral repertoire, *Elife*, 2018, **7**, e32605.

77 G. Wagner, On Some Movements and Reactions of Hydra ., *New Ser.*

78 L. M. PASSANO and C. B. McCULLOUGH, Co-ordinating systems and behaviour in hydra. I. Pacemaker system of the periodic contractions, *J. Exp. Biol. 41 643-664, 1964*, 1964, 643–664.

79 S. X. Guo, F. Bourgeois, T. Chokshi, N. J. Durr, M. A. Hilliard, N. Chronis and A. Ben-Yakar, Femtosecond laser nanoaxotomy lab-on-a-chip for in vivo nerve regeneration studies, *Nat Meth*, 2008, **5**, 531–533.

80 C. Hu, J. Dillon, J. Kearn, C. Murray, V. O'Connor, L. Holden-Dye and H. Morgan, NeuroChip: A Microfluidic Electrophysiological Device for Genetic and Chemical Biology Screening of Caenorhabditis elegans Adult and Larvae, *PLoS One*, , DOI:10.1371/journal.pone.0064297.

81 J. N. Stirman, M. Brauner, A. Gottschalk and H. Lu, High-throughput study of synaptic transmission at the neuromuscular junction enabled by optogenetics and microfluidics, *J. Neurosci. Methods*, 2010, **191**, 90–93.

82 V. Miralles, A. Huerre, F. Malloggi and M.-C. Jullien, A Review of Heating and Temperature Control in Microfluidic Systems: Techniques and Applications, *Diagnostics*, 2013, **3**, 33–67.

83 J. H. Jung, C. Han, S. A. Lee, J. Kim and C. Yang, Microfluidic-integrated laser-controlled microactuators with on-chip microscopy imaging functionality, *Lab Chip*, 2014, **14**, 3781–3789.

84 C. E. Juliano, H. Lin and R. E. Steele, Generation of Transgenic Hydra by Embryo Microinjection, 2014, e51888.

85 J. Wittlieb, K. Khalturin, J. U. Lohmann, F. Anton-Erxleben and T. C. G. Bosch, Transgenic Hydra allow in vivo tracking of individual stem cells during morphogenesis, *Proc. Natl. Acad. Sci.*, 2006, **103**, 6208–6211.

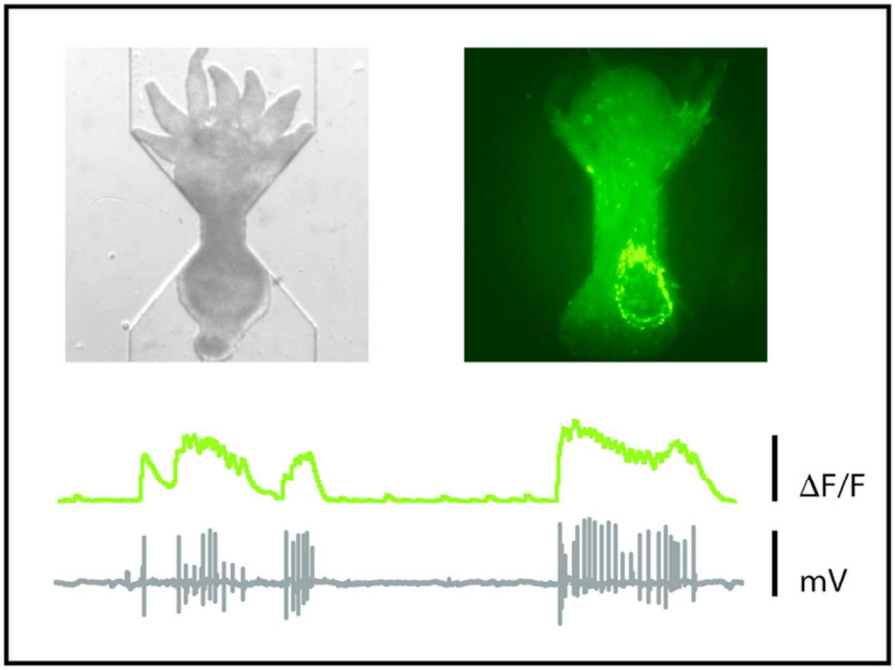

Microfluidic devices allow scalable and customizable solutions for multi-modal interrogation of these soft, deformable *Hydra*.

68x77mm (300 x 300 DPI)